IOPscience iopscience.iop.org

Home Search Collections Journals About Contact us My IOPscience

Synthesis of individual single-walled carbon nanotube bridges controlled by support micromachining

This article has been downloaded from IOPscience. Please scroll down to see the full text article.

2007 J. Micromech. Microeng. 17 603

(http://iopscience.iop.org/0960-1317/17/3/024)

View the table of contents for this issue, or go to the journal homepage for more

Download details:
IP Address: 129.169.173.162
The article was downloaded on 07/02/2013 at 16:48

Please note that terms and conditions apply.

J. Micromech. Microeng. **17** (2007) 603–608 doi:10.1088/0960-1317/17/3/024

Synthesis of individual single-walled carbon nanotube bridges controlled by support micromachining

Alain Jungen[1], Stephan Hofmann[2], Jannik C Meyer[3], Christoph Stampfer[1], Siegmar Roth[3], John Robertson[2] and Christofer Hierold[1]

[1] Micro and Nanosystems, ETH Zurich, 8092 Zurich, Switzerland
[2] Department of Engineering, University of Cambridge, Cambridge CB3 0FA, UK
[3] Max Plank Institute for Solid State Research, 70569 Stuttgart, Germany

E-mail: alain.jungen@micro.mavt.ethz.ch

Received 5 November 2006, in final form 16 December 2006
Published 16 February 2007
Online at stacks.iop.org/JMM/17/603

Abstract
Single-walled carbon nanotubes (SWNTs) were directly grown onto poly-crystalline silicon grids by catalytic thermal chemical vapour deposition. We demonstrate that simple micromachining of the catalyst-covered support can influence the number, location and alignment of suspended SWNTs. Sharp apexes formed by over-etching circular microstructures enable the scalable, cost-efficient formation of mostly individual, straight SWNT bridges, as verified by Raman scattering and electron diffraction.

1. Introduction

Controlling the interface between top–down microstructuring and the bottom–up synthesis of nano-scale building blocks, such as single-walled carbon nanotubes (SWNTs), is a crucial factor for the economic and scalable design of novel device architectures. A very high Young's modulus, thermal conductivity and current-carrying capacity makes SWNT particularly attractive for applications in nanoelectronics [1–3] and nanosensors [4, 5]. The controlled fabrication of individual suspended SWNTs is thereby desirable to fully exploit their intrinsic properties since interactions with other nanotubes or the underlying substrate can be excluded [6, 7]. Suspended SWNT-based systems also emanate, e.g., tuneable electromechanical resonators [8] or displacement sensors [9].

Catalytic chemical vapour deposition (CVD) of freestanding SWNTs has been demonstrated between nano-scale silicon oxide pillars [10] or textures [11]. However, neither precise alignment could be achieved nor SWNT bundling could be avoided as curved nanotubes were observed to randomly attach to neighbouring pillars. Surface-bound CVD allows control of nanotube alignment via external parameters such as electric fields, gas flow or substrate step-edges [12–17]. Tip-to-tip growth under an electric field has been demonstrated [18]; however, a large tip spacing of more than 5 μm resulted in curly nanotube bridges. Rapid thermal annealing was reported to create a convection flow thereby lifting the nanotubes up and causing them to float in the direction of the gas flow [19]. To date, economic large-scale device integration of SWNTs is hindered by the lack of reproducible control of the SWNT location and orientation orientation [20–22].

In this paper, we demonstrate the suitability of MEMS technology as a placeholder for the direct integration of suspended SWNTs. The driving force of this proposal is the previous observation of a simple SWNT bridge formation mechanism by which the nanotube is waving during its growth and attaching to the nearest support boundary [10, 23]. This implies that the support geometry should directly impact the directional bridging of SWNTs without the need of electric fields, strongly directed gas flows or a separate catalyst pre-patterning step. Furthermore, the ability to control the tube location and number is investigated in the present study.

2. Experimental detail

SWNT bridges were synthesized by catalytic thermal CVD in a low pressure furnace which can be operated to a base pressure of 10^{-5} mbar. Prior to the CVD growth, microchips were

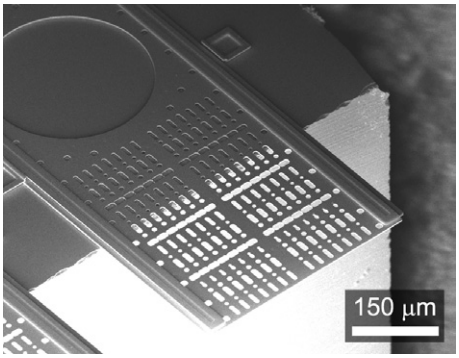

Figure 1. SEM image of a silicon microchip containing a surface micromachined grid slit off the chip edge.

fabricated by surface micromachining of releasable 1.5 μm thick poly-crystalline silicon (poly-Si) layers [24]. After their release, the poly-Si layers were uniformly coated with a bi-metallic thin film of 8 nm Al and 1 nm Ni in a sputter system. The film thickness was monitored *in situ* by a quartz crystal microbalance. The chips were transferred in air and subjected to a hydrogen pre-treatment at 200 mbar and 850 °C for 10 min to allow the reduction of nickel oxides and formation of Ni islands. The latter serve as catalytic seeds for the growth of SWNTs under methane and hydrogen (3:1) at 200 mbar and 850 °C during 15 min. Heating and cooling were performed under vacuum and the chamber was opened only after cooling to at least 250 °C.

The samples were characterized by scanning electron microscopy (SEM, Zeiss Ultra 55 operated at 5 kV) and transmission electron microscopy (TEM, Philips CM200 microscope operated at 120 kV). Electron diffraction (ED) patterns were recorded on a Zeiss 912 Ω microscope at 60 kV. Raman spectra were recorded on a WITec CRM 200 using the frequency-doubled Nd:YAG green laser line of 532 nm delivered through a single-mode optical fibre. This type of fibre supports only a single transversal mode which can be focused to a diffraction-limited spot size of about 400 nm (100X objective, NA = 0.8). The backscattered light was cut by a super-notch filter and focused into a 50 μm pinhole. The spectrometer was equipped with a Peltier-cooled charge coupled device (CCD) camera. Precise positioning of the sample under the laser spot was achieved with piezoelectric actuators with a travel range of 200 × 200 × 20 μm^3 in x, y and z, respectively. A calibration of the system was reported elsewhere [25].

3. Results and discussion

3.1. Horizontal growth and aligned bridges

Our study of SWNT bridge formation is based on the surface micromachined chip shown in figure 1 [26]. A poly-Si grid containing holes of different sizes and shapes is linearly guided by anchors. Upon release, the grid was moved over the chip edge to result in a partly freestanding structure [27]. This allows us to compare a range of hole geometries at one CVD exposure and as-grown SWNT to be subsequently analysed in the original growth environment, in particular by TEM which requires a transmissive electron path through the sample.

Figure 2(*a*) shows that the catalytically seeded SWNTs preferentially bridge over the shorter gap (1.5 μm wide) of a rectangular hole. The majority of the SWNTs is aligned normal to the hole edge and appears taut and straight. We want to emphasize that no electrical field was applied during growth. Also, the CVD was performed under static pressure, hence there was no gas flow. Several *in situ* thermocouples and separately addressable temperature controllers ascertained an equal temperature distribution in the CVD chamber. The poly-Si grid was highly doped ($n = 10^{19}$ cm^{-3}), thus charge trapping and local electrical fields can be excluded. We therefore suggest that the directionality in SWNT bridging is due to a simple nearest neighbour attachment.

SWNTs nucleate on the surface of individual catalyst particles, which typically remain on the substrate (root growth) [28, 29]. At the initial stages of growth, the SWNT body grows away from the substrate and with increasing length is subjected to thermal waving [30]. The SWNT thereby remains anchored at its nucleation point; however, the catalyst particle itself dynamically deforms during the continuous catalytic gas decomposition and carbon formation/incorporation [31]. Once the waving end of a SWNT comes close to the substrate, such as the opposing hole edge (figure 2(*a*), it is proposed that van der Waals interactions provide a strong adhesion, tightening and straightening to the now suspended nanotube [32].

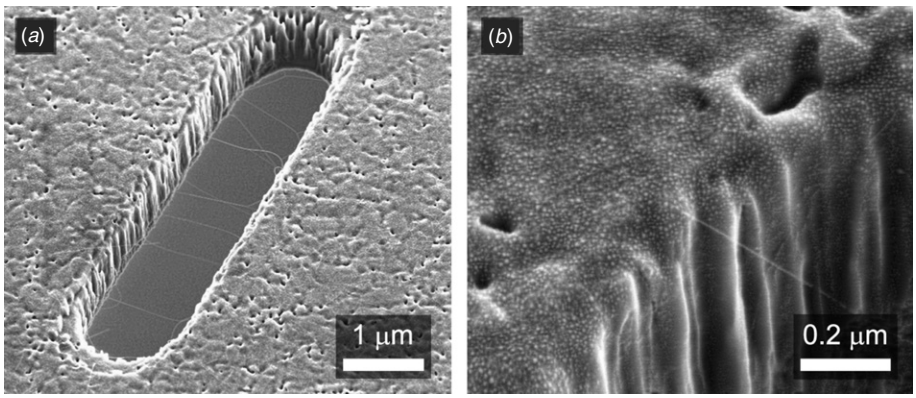

Figure 2. (*a*) SEM of a rectangular hole from the surface micromachined grid with aligned SWNT bridges. (*b*) Zoomed SEM image showing catalytic Ni particles and a SWNT bridge.

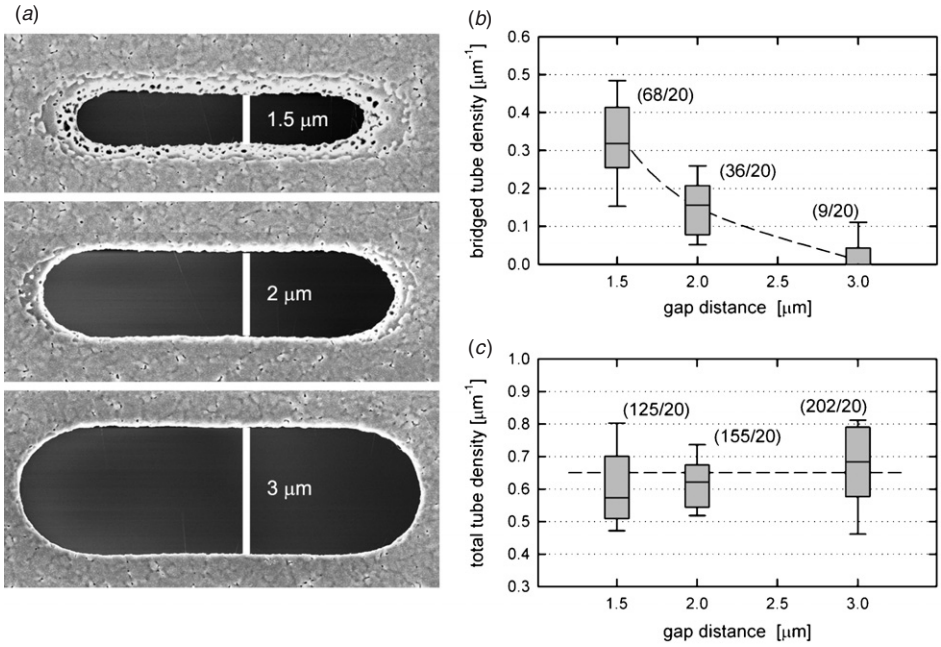

Figure 3. (*a*) SEM of rectangular holes of different gap sizes, (*b*) tube bridge density across different gap sizes. Figures in parenthesis indicate the number of measured tubes which successfully bridged over the gaps (tube bridges/gaps). (*c*) Total tube density in the same gaps. Figures in parenthesis indicate the number of measured tubes grown inside the gaps but which did not necessarily lead to a bridge (tubes/gaps).

Figure 2(*b*) shows a close-up SEM image of a SWNT bridge. The Ni catalyst islands are visible, uniformly covering the poly-Si surface. It can be seen that for the given CVD conditions the catalyst efficiency is low, i.e. the Ni island density is far higher that the SWNT density. The catalyst efficiency can be increased by optimizing catalyst film thickness and pre-treatment together with the carbon feedgas concentration and (reactive) dilution. However, a high catalyst efficiency results in vertically aligned SWNT forests due to van der Waals (tube–tube) interactions [33, 34], which is detrimental here regarding the desired lateral SWNT bridging.

For the given CVD conditions, figure 3(*b*) shows the influence of a gap-size variation between 1.5 μm and 3 μm on the number of crossing SWNT. The data are based on 60 highly resolved SEM images showing one hole at a time. All holes were on the same chip and thus were exposed to identical experimental conditions. The tube density is determined by taking the number of tubes divided by the hole's perimeter. Very occasional bridging was observed for trench sizes > 3 μm. There is a clear trend of increasing SWNT bridge formation for reduced gap size. We emphasize that the decreasing bridge density for increasing gap sizes is related to the reduced probability for growing longer nanotubes. This result is strongly recipe-dependent as larger gaps (about 20 μm or more) have been spanned in other experimental conditions [32, 35]. The plot in figure 3(*c*) shows that the SWNT density mainly relates to the catalyst efficiency and hence is not affected by the variation in gap size. We recall that the absolute number of suspended SWNTs strongly depends on the given CVD conditions. Given the relative trend of figure 3 we demonstrate control of the number of SWNT bridges by surface micromachining of the catalyst support.

3.2. Towards individual bridges

In the present section, we discuss the possibility of localizing the growth of individual tubes between two adjacent tips. Figure 4 shows three suspended SWNTs across a trench defined by a tip pair at the technological limit for standard surface micromachining. The shape has been designed based on the previous results, namely by alternating the gap spacing between 12 μm and 2 μm to force SWNT growth only between the small gaps without the need of masking the catalyst. Figure 4(*c*) shows a Raman map of the suspended SWNTs. The image was obtained by integrating the SWNT-specific Raman signatures, i.e., the radial breathing modes in the range from 80 to 350 cm^{-1} and the tangential (G) mode at around 1592 cm^{-1} as shown in figure 4(*d*). Raman scattering is resonant [36] and at a fixed excitation energy of 2.33 eV only two of the three crossing SWNTs could be seen at regular experimental conditions [37]. The SWNT diameter can be derived by $d = c_1/(\omega_{\mathrm{RBM}} - c_2)$ with $c_1 = 214$ nm cm^{-1} and $c_2 = 19$ cm^{-1} [38] and ω_{RBM} denoting the radial breathing mode frequency. We find $d = 1.43$ nm whereas no indication could be made for the neighbouring SWNT bridge as no ω_{RBM} was found. No defect-induced D-band signal at around 1350 cm^{-1} was observed, which is indicative for a good SWNT crystallinity. The Raman map displayed in figure 4(*c*) has been obtained by integrating over the longitudinal optical phonon mode of the poly-Si material. Both images can be overlaid as they picture the same structure. There is no doubt about the origin of these Raman features as the freestanding sample geometry does not suffer from any background signal.

The minimum feature size for the structures shown in figure 4 is about 2 μm. It should be noted that the lateral resolution of the MEMS technology was three orders of

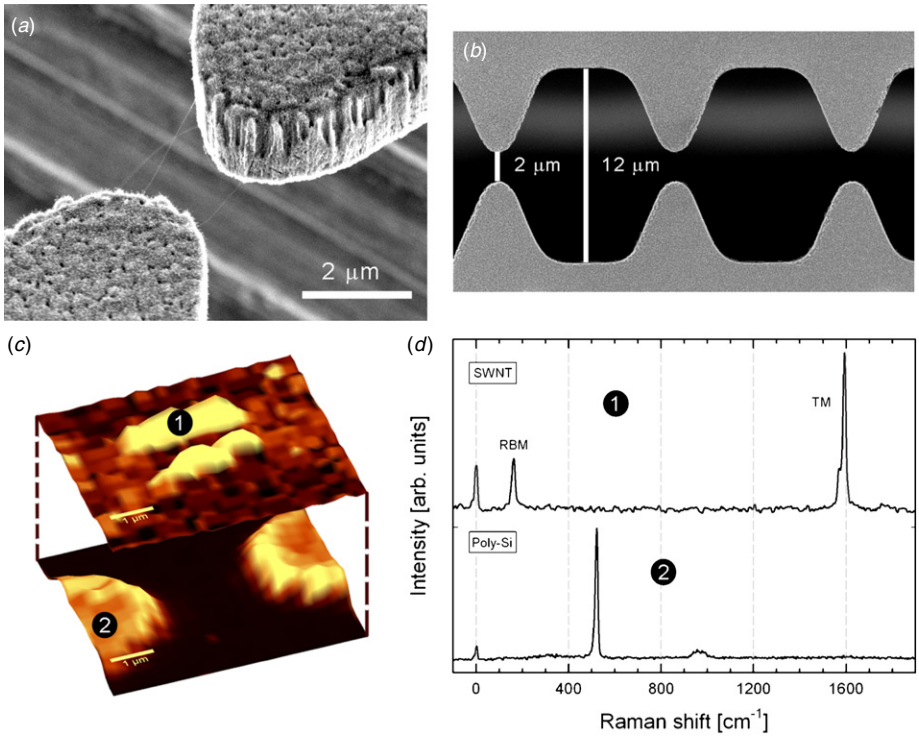

Figure 4. (*a*) SEM image of three SWNTs spanned between a pair of closely spaced poly-Si tips. (*b*) Demagnified SEM from (*a*) to show the tip definition. (*c*) Raman image of the same tip pair as shown in (*a*). (*d*) Representative snapshots showing SWNT and poly-Si-specific phonon modes in the Raman shift.

(This figure is in colour only in the electronic version)

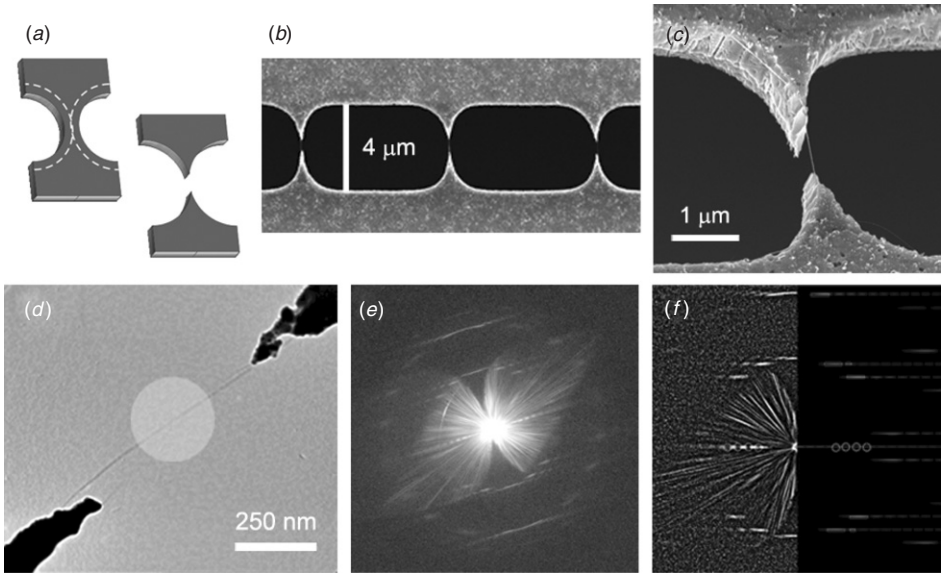

Figure 5. (*a*) Schematic of sharp tip formation from over-etching, (*b*) SEM image of a series of sharp tips, (*c*) SEM image of a SWNT which spanned over the pre-defined tips and (*d*) its corresponding TEM image. (*e*) ED pattern from the area indicated by the grey circle in (*d*). (*f*) High-pass filtered and rotated diffraction pattern (left) and simulated diffraction pattern of a (17, 10) SWNT (right). The boxes mark streaks in the pattern, the circles mark minima in the equatorial line. By comparing all nearby indices we verify that only the (17, 10) pattern matches the experimental one.

magnitude larger than the diameter of the SWNTs. We improved the lateral resolution of the micromachined tips by over-etching two initially circular holes to obtain two sharp adjacent tips defining a gap as shown in figure 5(*a*). Over-etching can be achieved by a controlled poly-Si oxidation and a subsequent acidic wet-etch. The distance between the two adjacent tips is below 1 μm. Crystal grains and their boundaries from the poly-crystalline material influenced the shape of the tip upon over-etching as can be seen in figure 5(*d*). Some nanotubes can be found attached to the sidewalls of the

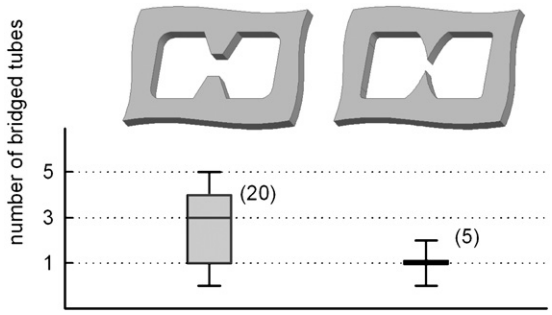

Figure 6. Box plot of two different tip apex geometries. Figures in parenthesis indicate the number of measured tip pairs. The ultra-sharp tips have a mean number of spanned SWNT of 1 tube per tip pair.

microstructures. As these additional SWNTs do not span across the gap, the system yield defined by individual crossing SWNTs is not affected.

The synthesis of straight nanotubes over a relatively short distance (∼800 nm) integrated into freestanding thin film microstructures allows for transmission electron investigations. Figures 5(*c*) and (*d*) show a TEM image and the corresponding electron diffraction pattern of an as-grown SWNT between the tips of the microstructure. Our ED analysis is described in detail in [39]. In short, the electron beam is limited to an area of 250 nm in diameter by the demagnified image of the condenser aperture. The illumination angle in the Koehler illumination condition is set to 0.16 mrad, the energy filter to 25 eV and the diffraction pattern is recorded on image plates with an exposure time of 4 min. Electrons scattered at the condenser aperture lead to a shadow image of the sample structure together with the pattern. The fact that we can obtain a diffraction pattern at all shows that we have a straight, well crystallized nanotube with a constant chirality within the illuminated region. The high-pass filtered and rotated pattern is compared with simulated diffraction pattern in order to identify the chiral indices of the SWNT (figure 5(*f*)). In this example, only the pattern simulated for an individual (17, 10) SWNT matches the experimental one, while all other candidates (and also bundles or multi-shell nanotubes) can be unambiguously excluded. The (17, 10) SWNT has a diameter of 1.85 nm and a chiral angle of 21.5°. This particular tube has energy separations (with good Raman scattering efficiency) closest to the excitation line of $E_{33}^{S} = 1.932$ eV and $E_{55}^{S} = 2.928$ eV [40]. As these two values are off the resonant window of 2.33 ± 0.4 eV these transitions could not be observed in the Raman experiment and a Raman map of the tube shown in figure 5(*d*) could not be recorded.

Figure 6 gives a comparison between the standard tip pairs seen in figure 4 and the ultra-sharp tips investigated in figure 5. For the ultra-sharp tips, in most cases only one SWNT bridged on defined sites gives a remarkable device yield (one tube per gap). The reduction of the gap size combined with the sharpening of the tip apexes also appears to give straighter SWNTs. We suggest that the sharp tip apexes minimize potential SWNT bending and buckling related to the tube–support interactions [32]. Opposing sharp tips can clearly improve a SWNT alignment based on nearest-boundary attachment. Since our process does not rely on directional electric fields and gas flows, individual SWNTs can be aligned in multiple directions across 6 inch wafers in an off-the-shelf industrial LPCVD furnace. The surface micromachining can be adopted to different CVD conditions, thus the described method offers a simple universal way of integrating individual SWNTs into scalable device designs.

4. Conclusion

In conclusion, we demonstrated the controlled, lateral growth of SWNT bridges by catalytic thermal chemical vapour deposition directly onto micromachined poly-Si grids. The number, location and alignment of suspended SWNTs were controlled solely by support design without a catalyst pre-patterning. The SWNTs self-aligned in static CVD conditions based on thermal waving and a simple nearest-boundary attachment. Sharp adjacent tips achieved by over-etching circular microstructures allow a scalable integration of individual, straight SWNTs with multiple alignments into standard MEMS technology.

Acknowledgments

The authors would like to thank O Homan, B Babic, D Miller, V Bright and M Height for support and helpful discussions. Funding support from the Swiss National Science Foundation (grant no 200021-108059/1), the ETH Zurich (grant no TH-18/03-1) and from the EU project CANAPE is greatly acknowledged. SH acknowledges support from Peterhouse, Cambridge and the Royal Society.

References

[1] Bachtold A, Hadley P, Nakanishi T and Dekker C 2001 Logic circuits with carbon nanotube transistors *Science* **294** 1317
[2] Appenzeller J, Martel R, Derycke V, Radosavjevic M, Wind S, Neumayer D and Avouris P 2002 Carbon nanotubes as potential building blocks for future nanoelectronics *Microelectron. Eng.* **64** 391–7
[3] Javey A, Guo J, Wang Q, Lundstrom M and Dai H 2003 Ballistic carbon nanotube field-effect transistors *Nature* **424** 654–7
[4] Stampfer C, Helbling T, Obergfell D, Schöberle B, Tripp M K, Jungen A, Roth S, Bright V and Hierold C 2006 Fabrication of single-walled carbon-nanotube-based pressure sensors *Nano Lett.* **6** 233–7
[5] Nishio M, Sawaya S, Akita S and Nakayama Y 2005 Carbon nanotube oscillators toward zeptogram detection *Appl. Phys. Lett.* **86** 133111
[6] Wang F, Sfeir M Y, Huang L, Huang X M H, Wu Y, Kim J, Hone J, O'Brien S, Brus L E and Heinz T F 2006 Interactions between individual carbon nanotubes studied by Rayleigh scattering spectroscopy *Phys. Rev. Lett.* **96** 167401
[7] Meyer J C, Paillet M, Michel T, Moréac A, Neumann A, Duesberg G S, Roth S and Sauvajol J-L 2005 Raman modes of index-identified freestanding single-walled carbon nanotubes *Phys. Rev. Lett.* **95** 217401
[8] Sazonova V, Yaish Y, Üstünel H, Roundy D, Arias T A and McEuen P L 2004 A tunable carbon nanotube electromechanical oscillator *Nature* **431** 284
[9] Stampfer C, Jungen A, Linderman R, Obergfell D, Roth S and Hierold C 2006 Nano-electromechanical displacement

sensing based on single-walled carbon nanotubes *Nano Lett*. **6** 1449–53
[10] Homma Y, Takagi D and Kobayashi Y 2004 Suspended architecture formation process of single-walled carbon nanotubes *Nano Lett*. **4** 1025–8
[11] Shi J, Lu Y F, Wang H, Yi K J, Lin Y S, Zhang R and Liou S H 2006 Synthesis of suspended carbon nanotubes on silicon inverse-opal structures by laser-assisted chemical vapour deposition *Nanotechnology* **17** 3822–6
[12] Franklin N R and Dai H 2000 An enhanced CVD approach to extensive nanotube networks with directionality *Adv. Mater.* **12** 890–4
[13] Franklin N R, Wang Q, Tombler T W, Javey A, Shim M and Dai H 2002 Integration of suspended carbon nanotube arrays into electronic devices and electromechanical systems *Appl. Phys. Lett*. **81** 913–5
[14] Zhang Y, Chang A, Cao J, Wang Q, Kim W, Li Y, Morris N, Yenilmez E, Kong J and Dai H 2001 Electric-field-directed growth of aligned single-walled carbon nanotubes *Appl. Phys. Lett*. **79** 3155–7
[15] Jungen A, Pfenninger M, Tonteling M, Stampfer C and Hierold C 2006 Electrothermal effects at the microscale and their consequences on system design *J. Micromech. Microeng*. **16** 1633–8
[16] Huang X M H, Caldwell R, Huang L, Jun S C, Huang M, Sfeir M Y, O'Brien S P and Hone J 2005 Controlled placement of individual carbon nanotubes *Nano Lett*. **5** 1515–8
[17] Ismach A, Kantorovich D and Joselevich E 2005 Carbon nanotube graphoepitaxy: highly oriented growth by faceted nanosteps *J. Am. Chem. Soc*. **127** 11554–5
[18] Chiu C-C, Tai N-H, Yeh M-K, Chen B-Y, Tseng S-H and Chang Y-H 2006 Tip-to-tip growth of aligned single-walled carbon nanotubes under an electric field *J. Cryst. Growth* **290** 171–5
[19] Huang S, Woodson M, Smalley R and Liu J 2004 Growth mechanism of oriented long single walled carbon nanotubes using fast-heating chemical vapor deposition process *Nano Lett*. **4** 1025–8
[20] Smalley R E, Li Y, Moore V C, Price B K, Colorado R Jr, Schmidt H K, Hauge R H, Barron A R and Tour J M 2006 Single wall carbon nanotube amplification: en route to a type-specific growth mechanism *J. Am. Chem. Soc*. **128** 15824–9
[21] Reich S, Li L and Robertson J 2006 Control the chirality of carbon nanotubes by epitaxial growth *Chem. Phys. Lett*. **421** 469–72
[22] Hofmann S, Csanyi G, Ferrari A C, Payne M C and Robertson J 2005 Surface diffusion: the low activation energy path for nanotube growth *Phys. Rev. Lett*. **95** 036101
[23] Peng H B, Ristroph T G, Schurmann G M, King G M, Yoon J, Narayanamurti V and Golovchenko J A 2003 Patterned growth of single-walled carbon nanotube arrays from a vapor-deposited fe catalyst *Appl. Phys. Lett*. **83** 4238
[24] Bustillo J M, Howe R T and Muller R S 1998 Surface micromachining for microelectromechanical systems *Proc. IEEE* **86** 1552–74
[25] Jungen A, Stampfer C and Hierold C 2006 Thermography on a suspended microbridge using confocal Raman scattering *Appl. Phys. Lett*. **88** 191901
[26] Jungen A, Stampfer C, Hoetzel J, Bright V M and Hierold C 2006 Process integration of carbon nanotubes into micro electromechanical systems *Sensors Actuators* A **130–131** 588–94
[27] Jungen A, Stampfer C, Durrer L, Helbling T and Hierold C 2006 A method for enhanced analysis of specific as-grown carbon nanotubes *Phys. Status Solidi* b **243** 3138–41
[28] Zhu H W, Suenaga K, Hashimoto A, Urita K, Hata K and Iijima S 2005 Atomic-resolution imaging of the nucleation points of single-walled carbon nanotubes *Small* **1** 1180–3
[29] Sharma R, Rez P, Treacy M M J and Stuart S J 2005 *In situ* observation of the growth mechanisms of carbon nanotubes under diverse reaction conditions *J. Elec. Micros*. **54** 231–7
[30] Lin M, Tan J P Y, Boothroyd C, Loh K P, Tok E S and Foo Y L 2006 Direct observation of single-walled carbon nanotube growth at the atomistic scale *Nano Lett*. **6** 449–52
[31] Helveg S, Lopez-Cartes C, Sehested J, Hansen P L, Clausen B S, Rostrup-Nielsen J, Abild-Pedersen F and Norskov J N 2004 Atomic-scale imaging of carbon nanofibre growth *Nature* **427** 426–9
[32] Abrams Z R and Hanein Y 2006 Tube–tube and tube–surface interactions in straight suspended carbon nanotube structures *J. Phys. Chem*. B **110** 21419–23
[33] Hata K, Futaba D N, Mizuno K, Namai T, Yumura M and Iijima S 2004 Water-assisted highly efficient synthesis of impurity-free single-walled carbon nanotubes *Science* **306** 1362–4
[34] Cantoro M, Hofmann S, Pisana S, Scardaci V, Parvez A, Ducati C, Ferrari A C, Blackburn A M, Wang K-Y and Robertson J 2006 Catalytic chemical vapor deposition of single-wall carbon nanotubes at low temperatures *Nano Lett*. **6** 1107–12
[35] Huang L, White B, Sfeir M Y, Huang M, Huang H X, Wind S, Hone J and O'Brien S 2006 Cobalt ultrathin film catalyzed ethanol chemical vapor deposition of single-walled carbon nanotubes *J. Phys. Chem*. B **110** 11103–9
[36] Dresselhaus M S, Dresselhaus G, Jorio A, Souza A G and Saito R 2002 Raman spectroscopy on isolated single wall carbon nanotubes *Carbon* **40** 2043–61
[37] Jungen A, Popov V N, Stampfer C, Durrer L, Stoll S and Hierold C 2006 Raman intensity mapping of single-walled carbon nanotubes *Phys. Rev.* B **75** 041405(R)
[38] Maultzsch J, Telg H, Reich S and Thomsen C 2005 Radial breathing mode of single-walled carbon nanotubes: optical transition energies and chiral-index assignment *Phys. Rev.* B **72** 205438
[39] Meyer J C, Paillet M, Duesberg G S and Roth S 2006 Electron diffraction analysis of individual single-walled carbon nanotubes *Ultramicroscopy* **106** 176–90
[40] Popov V N and Lambin P 2006 Resonant Raman intensity of the totally symmetric phonons of single-walled carbon nanotubes *Phys. Rev.* B **73** 165425